

## Article

# Collaborative Indoor Positioning by Localization Comparison at an Encounter Position

Kohei Kageyama <sup>1,\*</sup>, Tomo Miyazaki <sup>1,\*</sup>, Yoshihiro Sugaya <sup>2</sup> and Shinichiro Omachi <sup>1</sup>

<sup>1</sup> Graduate School of Engineering, Tohoku University, Sendai 9808579, Japan; kohei.kageyama.p3@dc.tohoku.ac.jp (K.K.); machi@ecei.tohoku.ac.jp (S.O.)

<sup>2</sup> Faculty of Advanced Science and Technology, Ryukoku University, Otsu 5202194, Japan; ysugaya@rins.ryukoku.ac.jp

\* Correspondence: tomo@tohoku.ac.jp

**Abstract:** With the widespread use of smartphones, there is a surging demand for localization in indoor environments. The main challenges are the requirement of special equipment (e.g., a map database and Wi-Fi access points) and error accumulation for indoor localization. In this paper, we propose a novel collaborative indoor positioning method to reduce error accumulation. Estimated positions are corrected using the collaborator's positions when an encounter is detected by communication based on Bluetooth Low Energy (BLE). In addition, a map is obtained by taking photos of information boards. Therefore, the proposed method needs smartphones only; other equipment is not required. We obtained an accurate localization comparison using a machine learning model. The experimental results showed that the proposed method achieved reliable encounter communication in eight facilities. The collaborative localization method successfully enhanced position estimations. Specifically, the proposed method outperformed the existing baseline method by 13.0% in accuracy of indoor positioning.

**Keywords:** Bluetooth Low Energy; collaborative localization; encounter communication; indoor localization; particle filter



**Citation:** Kageyama, K.; Miyazaki, T.; Sugaya, Y.; Omachi S. Collaborative Indoor Positioning by Localization Comparison at an Encounter Position. *Appl. Sci.* **2023**, *13*, 6962. <https://doi.org/10.3390/app13126962>

Academic Editor: Andrea Prati

Received: 10 May 2023

Revised: 30 May 2023

Accepted: 6 June 2023

Published: 9 June 2023



**Copyright:** © 2023 by the authors. Licensee MDPI, Basel, Switzerland. This article is an open access article distributed under the terms and conditions of the Creative Commons Attribution (CC BY) license (<https://creativecommons.org/licenses/by/4.0/>).

## 1. Introduction

Nowadays, smartphones have become necessary devices in our daily lives. With their widespread use, every day applications are using our location. For instance, we can quickly navigate using an online service such as Google Maps. However, indoor navigation is limited, since Global Navigation Satellite System (GNSS) signals are attenuated in indoor environments. Furthermore, a comprehensive database of indoor maps needs to be developed.

The use of indoor location is critical in various industries. Thus, many methods have been developed for indoor localization. For example, there are localization methods using indoor image databases [1,2], lighting information of the environment [3], the magnetic field of the structure [4], the Received Signal Strength Indication (RSSI) from Wi-Fi access points, and Bluetooth Low Energy (BLE) beacons installed inside a building [5,6]. However, these methods require special equipment and fingerprinting maps, which need periodic system maintenance following environmental changes. Maintenance is a heavy burden for managers. Although there is a method that does not require special equipment [7], it accumulates localization errors estimated by Pedestrian Dead Reckoning (PDR), resulting in inaccurate localization. In summary, existing methods encounter two obstacles: the maintenance of special equipment and the accumulation of localization errors.

In this paper, we aim to solve these two problems. The proposed method is based on work in [7]. Specifically, the proposed method uses only smartphones to estimate positions in a map image taken from an information board. Thus, the requirement for special equipment is avoided.

In addition, the error accumulation is suppressed by collaborative indoor localization. Specifically, we propose a method to exchange estimated localization using Bluetooth Low Energy (BLE)-enabled smartphones when users encounter each other. As shown in Figure 1, either of the phones can estimate a more accurate location, and the other can correct its location using the encounter place detected by BLE. There exists methods using encounter communication [8,9]. However, these methods do not fully utilize the estimated locations, as explained in Section 2.2. The proposed method compares the accuracy of the estimated locations using a machine learning model. Then, the localization performance is improved by the comparison result.

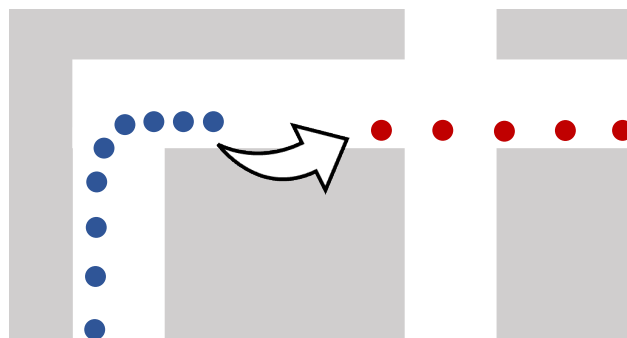


**Figure 1.** The key idea of collaborative localization. The inaccurate position (blue dot) is corrected using the more accurate encounter position (red dot).

The contributions of this paper are described in the following three points:

- A reliable encounter communication architecture using BLE-enabled smartphones.
- A model trained on synthesized data for comparing the localization of two users.
- A collaborative localization method by adjusting the localization parameters according to the comparison results.

The experiments were carried out at eight facilities. The results showed that the proposed localization comparison method achieved 83.0% localization accuracy. Furthermore, the proposed collaborative localization improved the baseline method by 13.0%.

## 2. Related Work

There are various approaches to realize indoor localization using a variety of modalities, such as Inertial Measurement Units (IMU), image analysis, and wireless communication. We briefly describe them.

### 2.1. Inertial Measurement Unit-Based Localization

Pedestrian Dead Reckoning (PDR) is a method of localization using IMU sensors such as accelerometers, gyroscopes, and magnetometers in the smartphone [10,11]. Smart-PDR [11] obtains the user's stride length using the relationship between stride and the magnitude of acceleration along the z-axis. The heading direction is determined by integrating the angular velocity obtained from the gyroscope and the value of the magnetometer.

Some methods process IMU sensor data with Deep Neural Networks (DNNs) such as CNNs to obtain the user's velocity vector [12–17]. RoNIN [14] uses accelerometer and gyroscope values from a smartphone as input. This method uses Visual Simultaneous Localization and Mapping (SLAM) trajectories as the training data to learn the trajectory of the user. Thus, the method uses velocity vectors to predict daily activities, such as walking, putting the device in a pocket, etc.

IMU-based methods suffer from error accumulation since localization is relative to the start position. Thus, the localization quality deteriorates significantly when the user walks a long distance. Therefore, the proposed method suppresses error accumulation by exploiting a new collaborative technique.

### 2.2. Localization with Indoor Maps

In order to reduce the localization error in IMUs or other approaches, there exist methods to utilize indoor maps [18,19]. These methods perform localization by combining indoor maps and map matching algorithms with a particle filter [7,20,21]. Map matching localizes the user’s position on the indoor map. Precisely, the methods predict the user’s walking trajectory on the indoor map by a particle filter using IMU data. The particles hold parameters such as position, orientation, and scale, which are successively updated by the velocity vectors obtained from the IMU. Each particle has a weight, representing confidence in the user’s location. Then, the position on the indoor map is calculated by the weighted average over the positions of the particles. Generally, the weight needs to be small if particles pass through the obstacles in the indoor map, such as a wall in the floor plan. Rormero et al. [20] calculated the overlap of obstacles with the trajectory. Then, the weight was decided according to the degree of the overlap.

The methods in [7,18–21] use indoor maps and map matching to reduce error accumulation. However, the localization fails if the error accumulation is too large and the indoor map is distorted. The proposed collaborative method solves this problem using the information from the other device.

### 2.3. Wireless-Based Localization

There is a localization approach using radio waves from Wi-Fi access points or Bluetooth beacons. The trilateration method identifies the position using three or more transmitters whose positions are known [22]. The position is an intersection of radio waves emitted by three transmitters. Localization by triangulation exploiting the Angle of Arrival (AOA) is also available [23]. However, the methods using radio waves are inaccurate since radio waves go through multiple paths in indoor environments due to wall reflection.

Several localization methods using Wi-Fi fingerprints have been developed [5,6]. These methods compile a database composed of RSSIs, which are related to indoor locations. Generally, the database is called the fingerprint. Localization is performed by matching an observed RSSI with the fingerprint. However, the construction of the fingerprint requires a large amount of human work.

There are methods of communicating with other users to improve the localization accuracy. Kloch et al. [8] corrected their location by merging the probability distributions for their own and others’ locations when users encountered each other. Qiu et al. updated the weights of a particle filter using the distance between their own device and other devices [9]. However, these methods only consider current locations. Previous locations are an informative resource to correct the current location. The proposed method analyzes various information in multiple steps to achieve a highly accurate localization.

## 3. Proposed Method

We propose a novel collaborative mechanism to reduce the cumulative error of localization by communicating between smartphones when two users encounter each other. As shown in Figure 2, the proposed method comprises three modules: encounter communication, localization comparison at the encounter location, and localization correction.

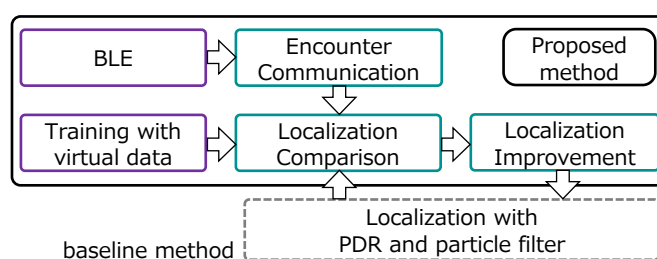


Figure 2. An overview of the proposed method.

We acquire walking data, stride length, and heading direction using SmartPDR [11]. Then, the indoor position is estimated by projecting the walking data to an indoor map obtained from the information board image. Inspired by localization using indoor maps [7], a particle filter is used to project walking data to the map image. If the encounter of users is detected, we compare the trajectories of estimated locations by a decision tree model trained on synthesized walking data. Finally, the positions are corrected according to the comparison result.

### 3.1. Baseline Localization Using a Particle Filter

We were inspired to adopt a particle filter by existing methods [24–26] with a particle filter for estimating the user’s position in a map image. Additionally, particle filters are used in a wide range of tasks, such as multiple target tracking [27], magnetic particle tracking [28], and wireless tracking of magnet position [29]. The Kalman filter is also a promising algorithm for the localization task [30,31].

We manually create the passage region, which consists of 0 or 1 values, from the image of the information board. Given a stride length  $l$  and a heading direction  $\theta_h \in [0, 2\pi]$ , one particle follows Equation (1) to update three parameters: the two-dimensional position  $(x, y)$  in the map image, the scale of the map  $mpp$  (meter-per-pixel), and the offset of the heading direction  $\theta_o$ . This converts the coordinates of the smartphone to the map image.  $\epsilon$  denotes noise from a normal distribution. Likewise, the sine function is used for updating  $y$ . Furthermore,  $mpp$  and  $\theta_o$  are updated by adding noise obtained from normal distributions. Finally, the position is defined as the average of the positions of all the particles. The number of particles is 2000. Particles will disappear if they are not in the passage region. Resampling is performed to keep the total number of particles constant. We followed the work in [7] to determine the number of particles. The proposed method removes particles if they are not in the passage regions. Thus, localization will fail if all the particles are removed at once. The experimental results verified that localization was performed successfully. All particles did not disappear at once. Therefore, the number of particles was sufficient.

$$x = x + \frac{l}{mpp + \epsilon_{mpp}} \cos(\theta_h - \theta_o + \epsilon_o) \quad (1)$$

### 3.2. Encounter Communication Using Bluetooth Low Energy (BLE)

Indoor localization using Bluetooth Low Energy (BLE) is an essential technology that is used in various indoor applications, such as emergency management [32], occupancy tracking [33], smart grids [34], and smart energy management [35] in buildings. In this paper, BLE is used to detect the user’s encounters and exchange the user’s localization performance, resulting in a realization of a collaborative localization.

A novel method of encounter communication is devised for two users using BLE. There are two modes in BLE: broadcasting and connection. Generally, the broadcast mode is used for encounter communication. However, we experimentally confirmed that the relationship between the RSSI and distance is more stable in the connection mode. Hence, the connection mode is used to realize encounter communication. In connection mode, the device has two roles: central and peripheral. The central mode scans packets and initiates a connection. The peripheral mode sends request packets and follows the central to exchange data. Communication is established only between the central and peripheral modes. In addition, devices cannot communicate with other devices if they have the same role. Therefore, we develop an application that operates both central and peripheral modes. The application chooses a suitable role dynamically. The flow of the proposed encounter communication is shown in Figure 3. The application has a unique number for each device. Here, the device operates the central mode at the beginning of the communication if it has a larger number than the other. Thus, communication can be prevented from being unstable due to the establishment of multiple communications between devices.

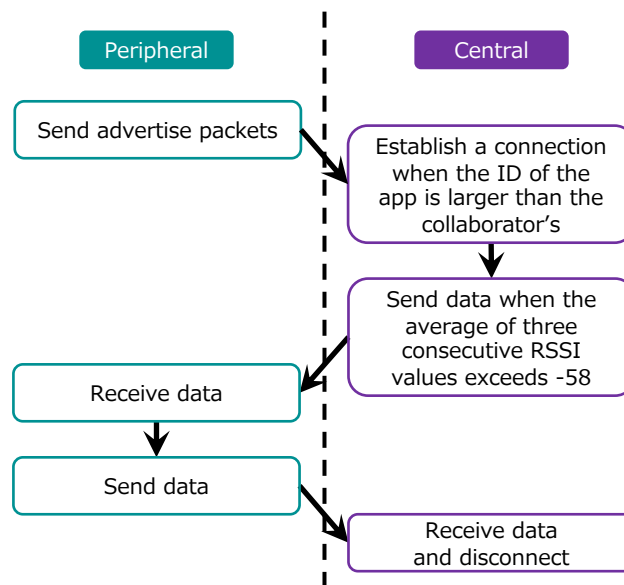


Figure 3. The flow of the proposed encounter communication.

An encounter is detected using the relationship between the RSSI and distance. Figure 4 shows an example of a relationship measured in the connection mode. A Google Pixel 4a was used. Specifically, we detect an encounter when an average of three consecutive RSSI values are larger than a threshold. The threshold is set to  $-58$  (dBm) in this study. For example, the encounter interval is from one to four meters in Figure 4. Communication is not established for 10 s after the previous communication to prevent multiple communications with the same collaborator immediately after the data exchange. In other words, the communication will not be re-connected for 10 s. Thus, an encounter will not be detected if the two devices re-encounter right after they first meet. Multiple and immediate re-encounters are not assumed in this work.

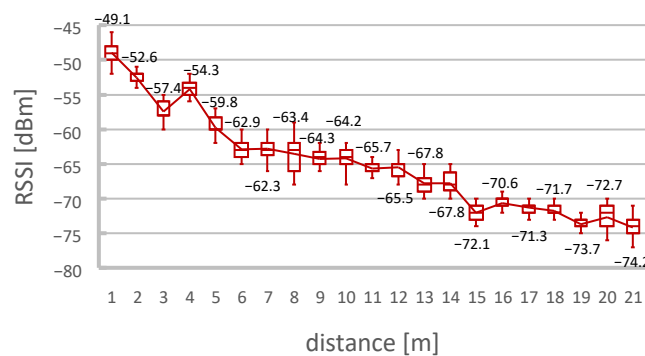


Figure 4. Relationship between the RSSI and distance. The value label is an average RSSI over 20 trials at each distance.

### 3.3. Localization Comparison

After an encounter is detected, the localization accuracies of two devices are compared using a machine learning model. Generally, models require large amounts of training data. However, actual walking data are difficult to obtain comprehensively. Therefore, we synthesize walking data and perform the baseline method to generate training data.

Data generation is described in Section 3.3.1. Furthermore, feature extraction and the machine learning model for localization comparison are described in Sections 3.3.2 and 3.3.4, respectively.

### 3.3.1. Generation of Walking Data

We generate walking data (stride length and heading direction per step) by connecting intersections in the map.

Firstly, as shown in Figure 5, a walking path is generated using an information board. We manually extract the passage region from the board image, resulting in a binary image (one if the pixels are in a passage region, zero otherwise). Intersections in the passage are defined by hand, and paths are created by connecting the intersections. We can dynamically create a walking path by finding a route connecting two randomly selected intersections.

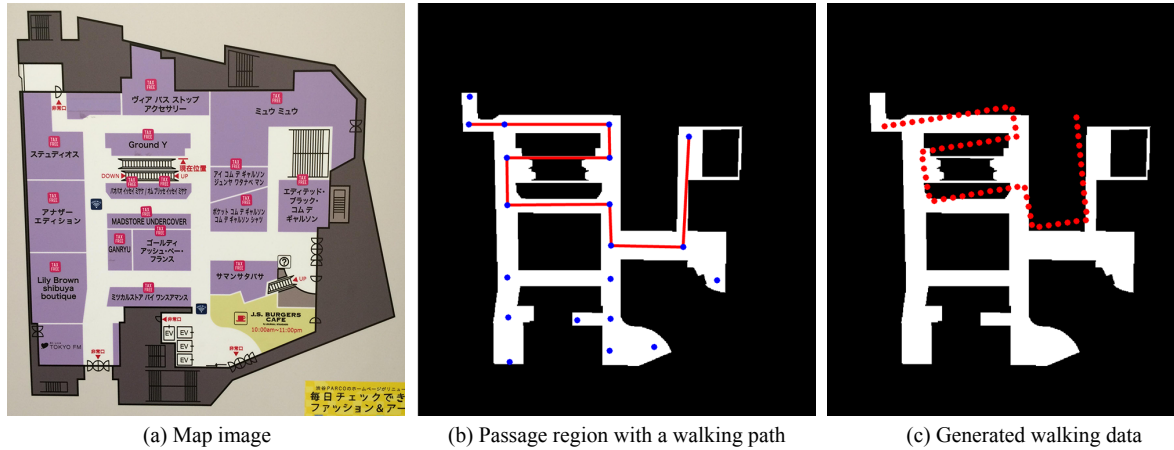


**Figure 5.** An example of walking data generation. The non-English terms in (a) are the store names.

Secondly, we generate walking data using a created walking path as shown in Figure 5c. Positions on the walking path are determined with the interval of 0.6 m, which is an approximate human stride length. Seven scales of the map  $mpp = 0.01 \times 1.5^\alpha \mid \alpha = 0, 1, \dots, 6$  are used to project the interval to the map image. In addition, random noise is generated in the positions since map distortion and PDR errors cause a discrepancy between the actual and generated walking paths.

Finally, sets of stride lengths and heading directions are obtained using the determined positions. For example, the stride length  $l_i$  at time  $i$  is defined as  $l_i = \|p_{i+1} - p_i\|_2 \times mpp$ , where  $p_i = (x_i, y_i)$  represents the position in the map image. Likewise, the heading direction is  $\theta_i = \arctan(y_{i+1} - y_i, x_{i+1} - x_i)$ .

### 3.3.2. Feature Extraction from Localization Process

We extract 15 features expressed in Table 1 from the localization process of the baseline method. Broadly, the features can be grouped into four categories. The features are developed by focusing on a position where a user makes a turn. We detect a turning position  $p_i$  from the walking data if Equation (2) is satisfied [36]. The turning position is useful for evaluating the localization quality. For instance, the localization quality is poor if there is a large gap between the turning position and the nearest intersection. Furthermore, disappearing particles are essential features. The presence of disappearing particles means there is a very low possibility that the device will be located at those certain positions, which indicates that the device is very likely passing through an obstacle. Moreover, large variations in the particle parameters indicate that a variety of particles are required to correct the localization. Since the results obtained by PDR are relative positions, errors accumulate as the number of steps increases.

$$\left| \frac{\theta_i + \theta_{i-1}}{2} - \frac{\theta_{i-2} + \theta_{i-3}}{2} \right| > 30 \tag{2}$$

**Table 1.** The features extracted from the localization process.

Features	Descriptions
Turns and intersections	<ul style="list-style-type: none"> <li>• Average distance from each turn to the nearest intersection</li> <li>• Maximum distance from each turn to the nearest intersection</li> <li>• Number of times an intersection exists within 1m of a turn</li> <li>• Number of times an intersection exists within 3m of a turn</li> <li>• Number of times no intersection exists within 1m of a turn</li> <li>• Number of times no intersection exists within 3m of a turn</li> </ul>
Disappeared particles	<ul style="list-style-type: none"> <li>• Number of particles disappearing per step</li> <li>• Whether all particles have disappeared or not</li> <li>• Number of steps in which over 40% of the have particles disappeared</li> <li>• Number of steps in which over 60% of the have particles disappeared</li> <li>• Number of steps in which over 80% of the particles have disappeared</li> </ul>
Statistics of particles	<ul style="list-style-type: none"> <li>• Standard deviation of position at the final location</li> <li>• Standard deviation of scale at all steps</li> <li>• Standard deviation of heading direction offset at all steps</li> </ul>
Others	<ul style="list-style-type: none"> <li>• Number of steps</li> </ul>

### 3.3.3. Evaluation Metric for Localization

Estimated positions are evaluated using a metric  $M$  defined in Equation (3). Specifically, we use the Dynamic Time Warping distance  $D$  [37] to measure the distance between the estimated positions  $S = \{(x_i, y_i) \mid i = 1, \dots, n\}$  and the ground truth (GT) position  $T = \{(x_i, y_i) \mid i = 1, \dots, n\}$ .  $T$  is created by selecting points on the walking path with a fixed interval, which divides the path equally. We used sampling points of the GT path to match estimated positions to appropriate points on the GT. For example, as shown in Figure 6, the estimated positions in the red dashed circle should be matched to the two points, respectively. If the GT path is used, the estimated two points will be matched to close points on the GT path, resulting in incorrect matches.  $N_{\text{match}}$  is the number of matching elements of the series  $S$  and  $T$ . A smaller metric is better.

$$M = \frac{D(S, T)}{N_{\text{match}}} \tag{3}$$

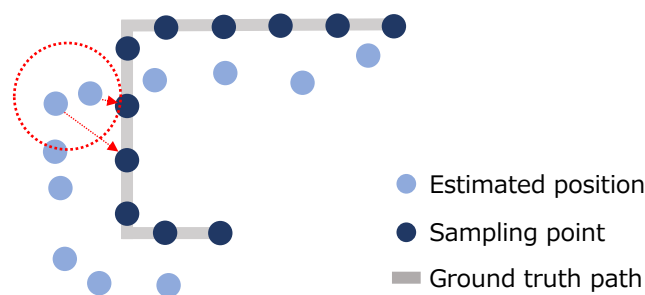


**Figure 6.** Evaluation metric using sampling points of the ground truth path.

### 3.3.4. Comparison Method Using Machine Learning

Localization qualities are compared by a decision tree model as shown in Figure 7. Specifically, we use a gradient boosting framework, LightGBM [38]. The effectiveness of the gradient-boosting machine (GBM) algorithm has been verified in a wide range of tasks, such as binary classification [39], multi-class classification [40,41], and fault detection [42]. Additionally, we considered the efficiency of the algorithm since a mobile device is used to run the model.

We compared two localization processes,  $A$  and  $B$ . The features are extracted from each process and concatenated to make input features for the model. The label value zero

is assigned to the input features if the metric of the process  $A$  is smaller than  $B$ . Therefore, the model is trained by solving a binary classification task. The output of the model is a value ranging from 0 to 1.

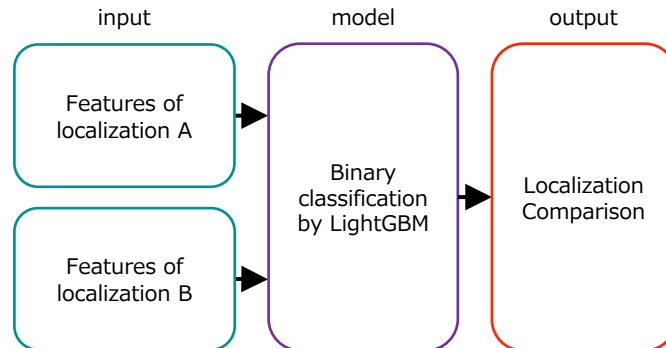


**Figure 7.** The flow of localization comparison.

The model is trained on only the synthesized walking data. Two localization processes are performed on the same map image and  $mpp$ . We allow no encounters between the processes. Thus, the model compares independent localization processes.

### 3.4. Collaborative Localization Correction

Particles are corrected using the encountered user’s position and the comparison model’s output. The two users are close to each other when an encounter is detected. Therefore, we can correct the localization of both encountered users by replacing the position of some particles  $(x, y)$  with the position of the collaborator  $(x_c, y_c)$ . Here, we assume that both devices use the same map for localization. Equation (4) is used to determine the number of particles to be corrected according to the comparison output  $o$ , which represents the collaborator’s localization quality against their own localization.  $N_{total}$  is the total number of particles in their own device. For example, when  $o = 0.2$ , 20% of the position of particles  $(x, y)$  are replaced with the collaborator’s position  $(x_c, y_c)$ .  $\sigma_{pos} = 1.5$  m is used to consider the deviation of the distance between users during the encounter (and positioning errors). Accordingly, the position of the particle is corrected by  $(x, y) = (x_c + N(0, \sigma_{pos}^2), y_c + N(0, \sigma_{pos}^2))$ .

$$N_{replace} = N_{total} * o \tag{4}$$

The offset  $\theta_o$  of particles is corrected, since the heading direction can deviate when a localization has significant errors. This offset is determined according to the initial heading direction on the map. Hence, we correct the offset using the offsets of previous particles. Specifically, the offset is updated by Equation (5). We update 50 % of particles at time  $i$ . The function med represents the median function.  $\bar{\theta}_{o,i}$  is the average offset in particles at time  $i$ . The average offset  $\bar{\theta}_{o,i}$  is used to suppress a drastic update.  $\sigma_{noise} = 2.0$  denotes the standard deviation.

$$\theta_{o,i} = \text{med}(\bar{\theta}_{o,1}, \dots, \bar{\theta}_{o,i-1}) + N(0, \sigma_{noise}) \tag{5}$$

## 4. Experiments

Three experiments were carried out to evaluate the proposed collaborative localization method, the encounter communication, and the localization comparison.

### 4.1. Datasets

We developed training and test datasets containing information map images and walking data (stride lengths and heading directions). The map images of twelve and eight facilities were obtained for training and test datasets, respectively.



The training dataset contained the synthesized walking data described in Section 3.3.1. We generated 50 walking data for each map image and scale *mpp*. Then, baseline localization was applied to the walking data ten times to extract the features of localization. Thus, there were 3500 sets of localization results for a map. Two results were selected randomly from the same map at the same scale to generate input features for the comparison model. Consequently, the training dataset contained 42,875 input features for each map. The comparison model was trained using the training dataset.

The test dataset was actual walking data obtained by a smartphone, a Google Pixel 4a, at eight facilities. As shown in Figure 8, there were two walking data properties in a map. The walking data included the time and position of the encounter, which was successfully detected by the proposed method. The walking paths in the map images were determined manually.

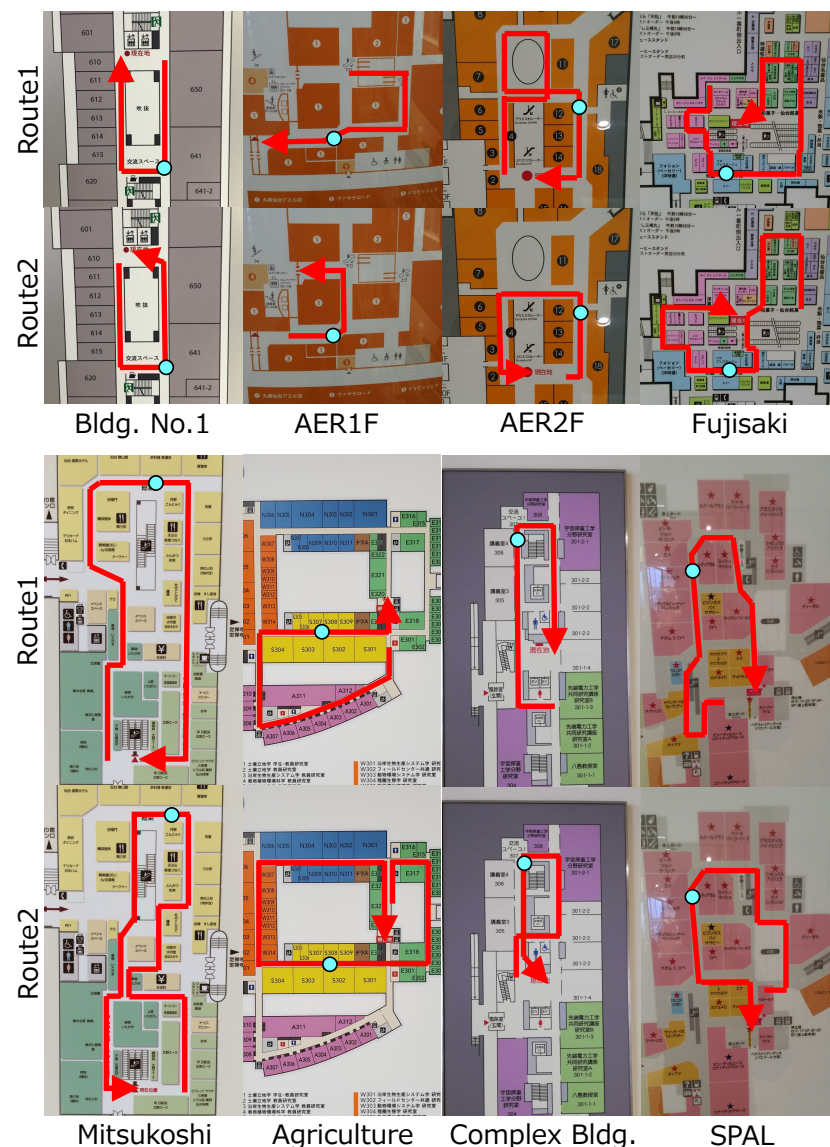


**Figure 8.** Test dataset. Red is a walking path. Cyan is an encounter position. The non-English terms in the maps are the room and store names.

#### 4.2. Evaluation on Localization

The proposed method was evaluated in 100 trials using each walking dataset. The evaluation metric for the localization is described in Section 3.3.3. There are two comparison methods for indoor localization using map images. The first comparison method is the

baseline method using PDR and particle filter described in Section 3.1. The second comparison method, Qiu’s method [9], improves the baseline method by modifying the weights of particles using encounter communication. When the standard deviation of the collaborator’s particles,  $\sigma_C$ , is within 10 m, the weight of the particle  $W_i$  with index  $i$  is updated by Equation (6).  $p_i$  is the position of the particle and  $l_C$  represents the estimated location of the collaborator at the encounter. The hyperparameters  $\mu_{BLE}$  and  $\sigma_{BLE}$  represent the average and standard deviation of distances between two devices measured by BLE. Values of  $d = 1.91$  and  $\sigma_E = 1.26$  were determined experimentally.

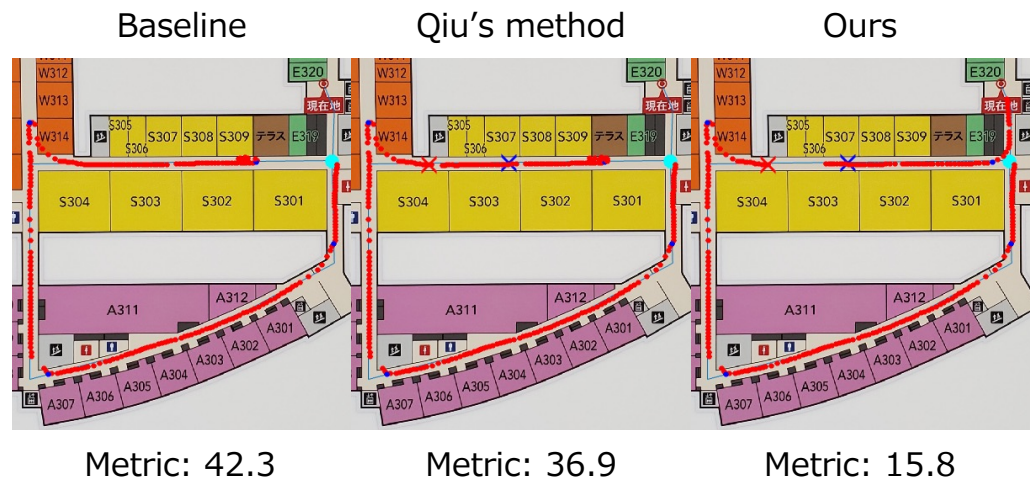
$$W_i = \exp\left(-\frac{(\|p_i - l_C\| - \mu_{BLE})^2}{2(\sigma_C + \sigma_{BLE})^2}\right) \quad (6)$$

Table 2 shows the localization results. The proposed method improved the baseline of the average metric by about 18 pixels. On the other hand, the improvement by Qiu’s method was about 2 pixels, which was much smaller than the proposed method. Qiu’s method did not sufficiently utilize the collaborator’s position when modifying the localization. The proposed method exhibited some slight degradations in accuracy, such as route 2 in Fujisaki and Mitsukoshi. Since the collaborator’s position was far from the encounter point, the particles were updated to the wrong positions.

**Table 2.** Average metric (error distance in pixels) in map images for indoor localization. Bold is the best result. Lower is better.

Facility	Walk	Baseline	Qiu [9]	Ours
Bldg. No. 1	1	21.4	<b>21.0</b>	22.3
	2	28.3	<b>28.1</b>	28.3
AER1F	1	93.5	90.9	<b>66.2</b>
	2	62.5	61.2	<b>57.2</b>
AER2F	1	100.4	97.5	<b>88.5</b>
	2	135.2	134.6	<b>112.1</b>
Fujisaki	1	184.8	178.0	<b>90.0</b>
	2	<b>25.0</b>	<b>25.0</b>	31.1
Mitsukoshi	1	58.7	54.4	<b>43.9</b>
	2	39.7	<b>38.1</b>	51.8
Agriculture	1	69.1	57.0	<b>34.4</b>
	2	30.2	28.9	<b>28.6</b>
Complex	1	44.6	44.5	<b>41.3</b>
	2	<b>44.7</b>	<b>44.7</b>	46.7
SPAL	1	95.0	118.7	<b>50.2</b>
	2	214.2	193.6	<b>173.6</b>
Average		78.0	76.0	<b>60.4</b>

Figure 9 shows an example of the correction for route 1 in Agriculture. The cyan dots are the start positions. The red and blue dots are the estimated position and the turning point, respectively. The red and blue cross marks are the detected encounter positions of the user and its counterpart, respectively. The proposed method correctly estimated the position after collaborative localization correction at the detected encounter. In contrast, the baseline method accumulated errors. Qiu’s method slightly modified the localization using the collaborator’s position. However, the effect of the modification was insufficient.



**Figure 9.** Results from Agriculture route 1. Red dots indicate the estimated positions. Cyan dots are starting position. Blue dots represent turns. Red and blue cross marks depict the detected encounters of the two uses. The non-English term in the map indicates the location of the map board in the physical facility.

4.3. Ablation Study on the Collaborative Localization Correction

We evaluated the two modules in the collaborative localization correction, updating the number of particles and the offset using Equations (4) and (5), respectively. Specifically,  $\sigma = 0.5$  was fixed to determine the number of particles. Furthermore, the offset was updated by adding a normal distribution:  $\theta_o = \theta_o + N(0, \sigma)$ .

Table 3 shows the improvement rates from the baseline method. Specifically, the improvement rate was calculated by  $(\text{Baseline} - \text{Ours}) / \text{Baseline}$ . The full proposed method achieved the highest improvement rate of 13.0%. The method using  $\sigma = 0.5$  achieved the highest improvement rate in route 2 of AER2F and Agriculture. However, there was significant deterioration, for example, for route 2 of Mitsukoshi. The method with  $\theta_o + N(0, \sigma)$  obtained slightly higher improvement rates than the full proposed method on some routes. On the other hand, there was a significant decrease at route 1 in Mitsukoshi. Figure 10 shows examples of the results. The heading directions significantly deviated in both methods before the encounter. The method with  $\theta_o + N(0, \sigma)$  accumulated error after the encounter, whereas the full proposed method successfully estimated the direction.

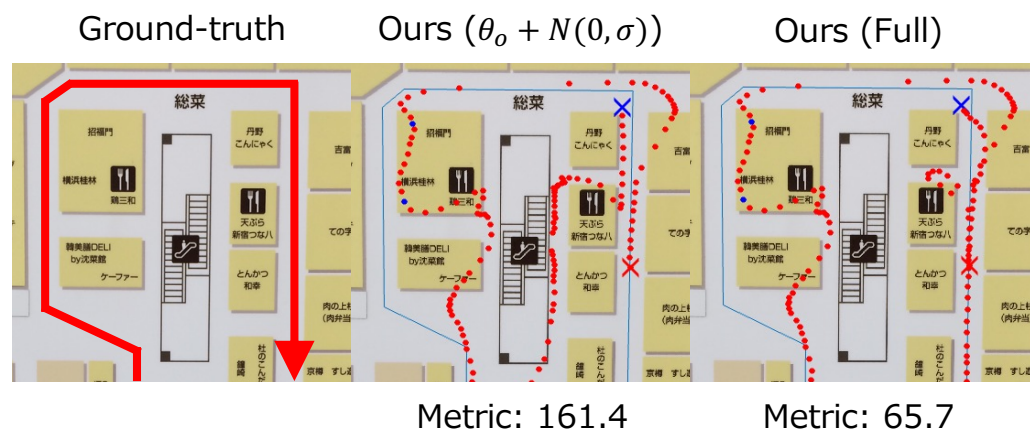


**Figure 10.** Ablation results for Mitsukoshi route 1. Red dots indicate the estimated positions. Blue cross mark depicts the detected encounter. The non-English term in the map indicates store names.

**Table 3.** Improvement rate (%) from the baseline by the ablation study. Bold highlights the best result. Higher is better.

Facility	Walk	Ours ( $\sigma = 0.5$ )	Ours ( $\theta_o + N(0, \sigma)$ )	Ours (Full)
Bldg. No. 1	1	−7.9	−4.7	−4.2
	2	<b>1.1</b>	0.4	0.0
AER1F	1	<b>31.6</b>	30.2	29.2
	2	1.1	4.3	<b>8.5</b>
AER2F	1	9.8	8.6	<b>11.9</b>
	2	<b>35.2</b>	5.6	17.1
Fujisaki	1	<b>51.4</b>	48.9	51.3
	2	−27.2	−17.2	−24.4
Mitsukoshi	1	17.5	12.9	<b>25.2</b>
	2	−138.0	−27.5	−30.5
Agriculture	1	48.5	50.1	<b>50.2</b>
	2	<b>33.8</b>	−1.7	5.3
Complex	1	<b>8.3</b>	7.0	7.4
	2	−9.4	−5.8	−4.5
SPAL	1	37.2	<b>48.0</b>	47.2
	2	<b>21.8</b>	13.4	19.0
Average		7.2	10.8	<b>13.0</b>

#### 4.4. Evaluation of Localization Comparison

The localization comparison model was trained on the training dataset using a cross-entropy loss function. The validation dataset was created by extracting one-quarter of the training dataset and the best model was determined by evaluating the validation dataset. Then, we evaluated the model using the walking data from the start to the encounter in the test dataset. We averaged the results obtained by cross-validation.

Table 4 shows that an accuracy of 0.83 was obtained on the test dataset. Accuracy was low in Building No. 1 and AER2F, where their localizations were highly accurate. Figure 11 shows examples of comparison pairs of localizations in AER2F. The comparison was correct when the metrics were considerably different. In addition, the number of disappearing particles significantly affected the comparison determination. Many particles disappeared in Figure 11a. The failed example had two close localizations in the metric. The incorrect result was produced by the features related to turns and intersections. Figure 11d had a smaller average distance from each turn to the nearest intersection than Figure 11c.

**Table 4.** Accuracy of the localization comparison.

Facility	Accuracy (%)
Bldg. No. 1	0.66
AER1F	1.0
AER2F	0.68
Fujisaki	0.77
Mitsukoshi	0.96
Agriculture	1.0
Complex	0.78
SPAL	0.79
Average	0.83

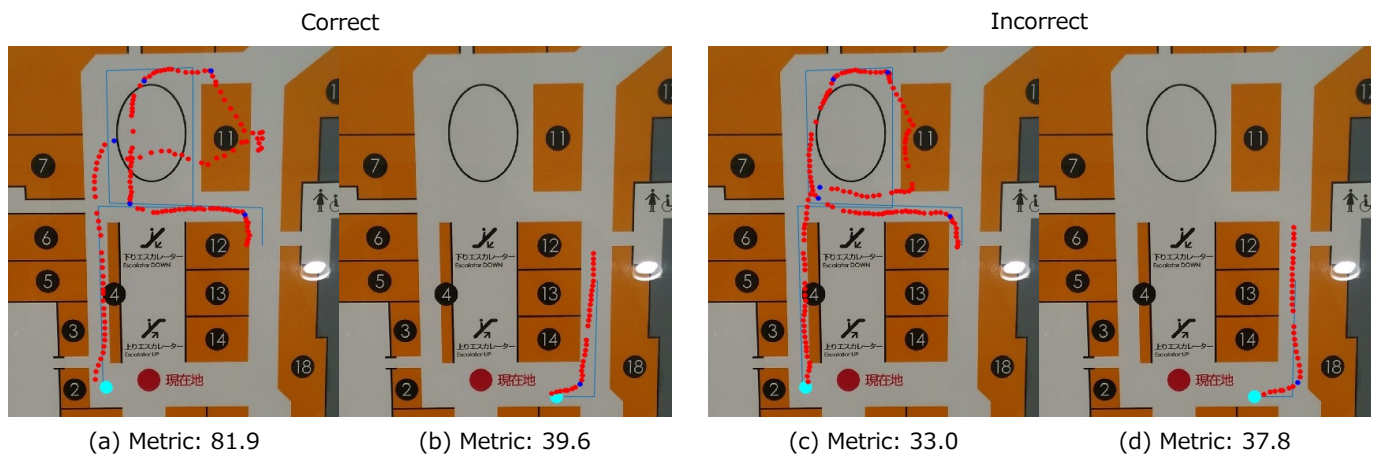


**Figure 11.** Results of localization comparison in AER2F. Red and cyan dots indicate the estimated and starting positions, respectively. Blue dots depict the detected turns. Light blue line is the ground truth path. The non-English term in the map indicates the escalator.

Figure 12 shows the importance of the features of the comparison model. The importance represents the contribution of each feature to decreasing the loss function. The importance was calculated using the validation dataset. The input features to the model consisted of two localizations. Then, we averaged the corresponding features to obtain the importance of the 15 features.

Generally, the importance  $I$  at a node of a decision tree can be calculated by  $I = rL - r_1L_1 + r_2L_2$ , where  $L$  and  $r$  represent the loss value at the node and the ratio of the sample size at the node to the total sample size, respectively. Likewise,  $L_1$  and  $r_1$  are of the left leaf of the node. In this work, binary cross-entropy was used to calculate the loss value. Thus, the importance of a feature  $f$  is the total importance at all nodes using  $f$ . If the importance is larger, the feature significantly reduces the loss value.

The results showed that the average distance from each turn to the nearest intersection was the most important feature. The proposed method detects the user's turn positions, and then the distance is measured. Intuitively, the localization performance is high if the predicted turn position is close to the GT intersection. Therefore, the feature is a critical metric for localization performance.

Figure 13 shows the average outputs of the comparison model for correct and incorrect cases. Values were unavailable if there were only correct cases. For simplicity, the output was subtracted from 1 if it exceeded 0.5. Thus, a smaller value indicates a higher confident estimation. In contrast, a value close to 0.5 means an ambiguous estimation. The results showed that the model was more confident for correct than incorrect instances. The outputs in Building No.1 were less confident, since both correct and incorrect were close to 0.5. In fact, the comparison accuracy was the lowest, 0.66, among the facilities. Thus, the model did not make a significant mistake in its estimation on this map.

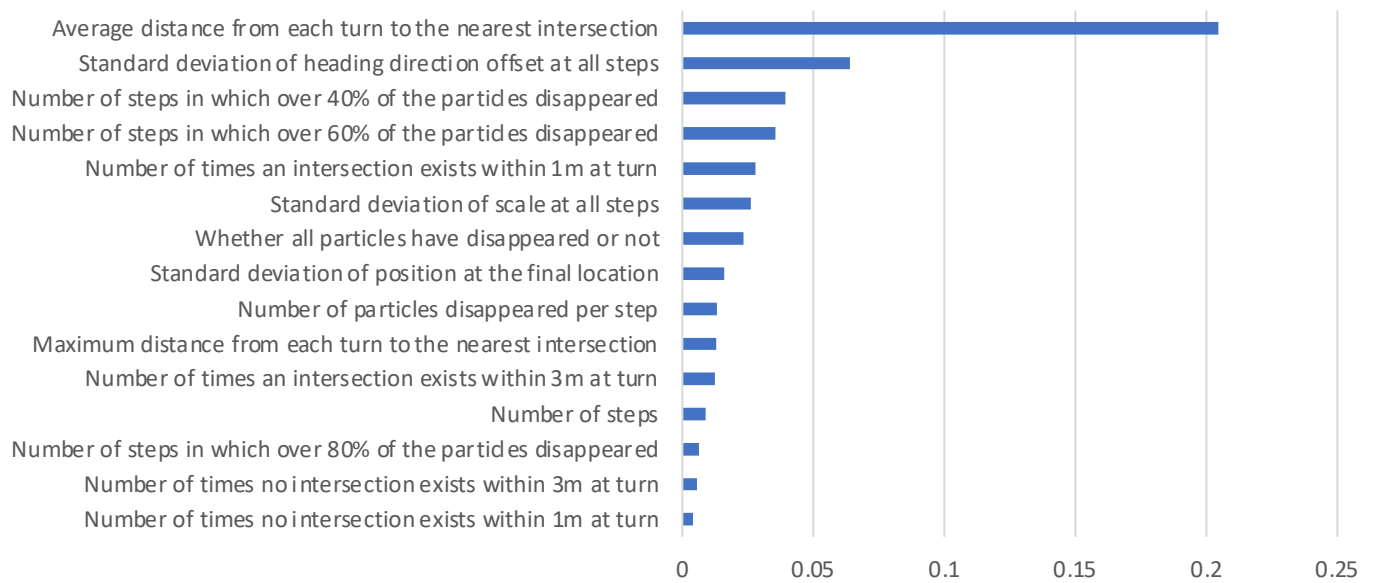


Figure 12. Importance of features in the localization comparison model.

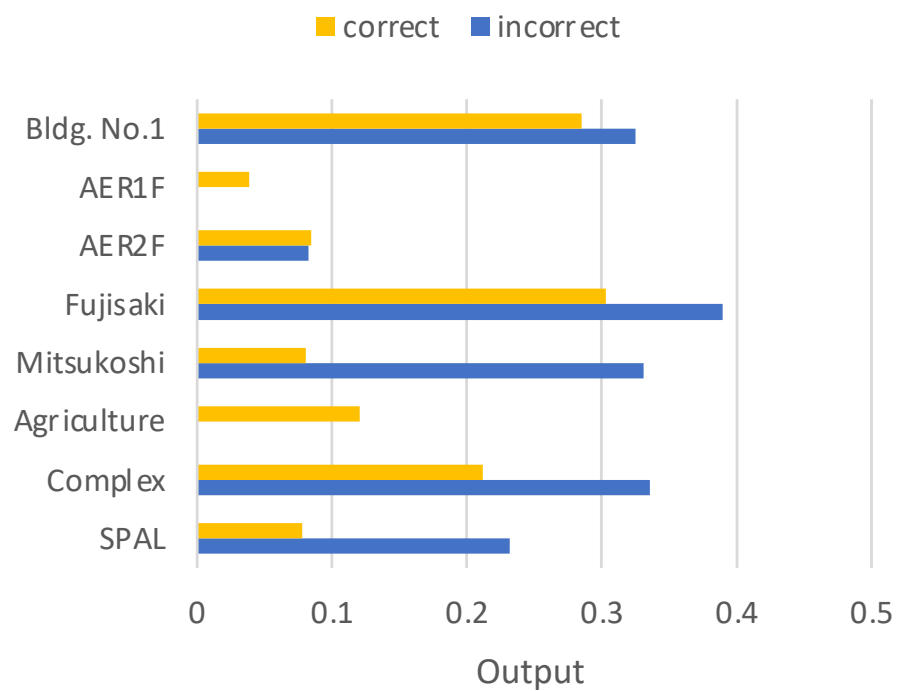


Figure 13. Average output of the localization comparison model.

#### 4.5. Evaluation of Encounter Communication

The encounter communication was evaluated on two facilities in the test dataset. As shown in Figure 14, two users moved step by step. Then, the distance was measured between the users when an encounter was detected. Ten trials were conducted. The amount of data exchanged at the encounter communication was 500 Bytes.

Table 5 shows the results of the encounter communication. Although the encounter communication failed once, the proposed method successfully detected encounters at an average distance of 1.9 m. The detected distance in Building No.1 was smaller than that

for the Complex building. The surrounding walls in the route in Building No.1 are partly made of glass. Thus, the radio waves went through the glass and communication was detected at a close position due to fewer reflected waves.

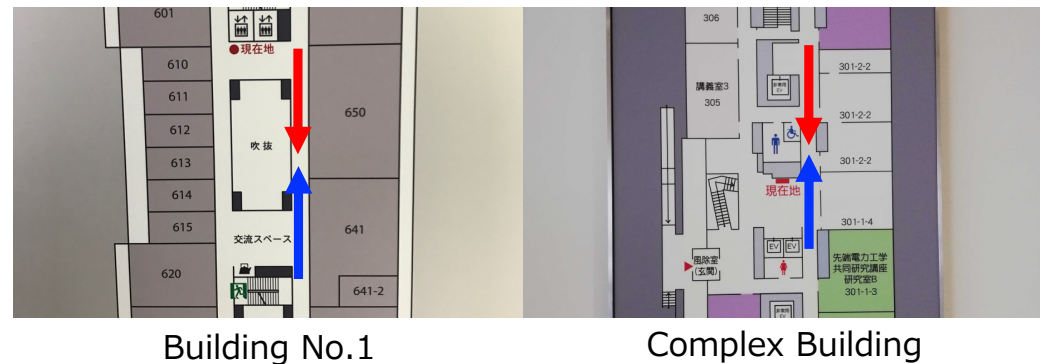


**Figure 14.** The walking paths (red and blue) for encounter communication. The non-English terms in the map indicate room names.

**Table 5.** Results of encounter communication.

	Bldg. No. 1	Complex Bldg.	Overall
Detection rate	0.90	1.00	0.95
Average distance (m)	1.26	2.57	1.91
SD. of distance (m)	0.87	1.29	1.26

## 5. Conclusions

In this paper, we proposed a novel collaborative localization using BLE-based encounter communication. In this encounter communication, an architecture that achieved communication of 500 Bytes was realized. Our method allows multiple communications to be established. We also developed a method to compare the localization of two devices. Virtual walking data were generated and we trained a decision tree model. In addition, we proposed a novel method for correcting the position and direction by using the output value of the comparison. The experimental results showed that the comparison model achieved an 83.0% accuracy for 16 routes at eight facilities. In addition, the proposed method improved the baseline method by 13.0% by appropriately using the collaborator's location.

The limitation of the proposed method is the manual analysis of map images taken from information boards. In this study, passage regions are manually extracted from the map images. Thus, an automatic method of passage extraction is necessary. A potential approach for automatic extraction is using semantic segmentation models, such as fully convolutional networks [43] and DeepLabv3+ [44].

**Author Contributions:** Conceptualization, K.K. and Y.S.; methodology, K.K.; software, K.K.; validation, K.K. and T.M.; formal analysis, K.K.; investigation, K.K. and Y.S.; resources, K.K.; data curation, K.K.; writing—original draft preparation, K.K. and T.M.; writing—review and editing, S.O.; visualization, K.K.; supervision, S.O.; project administration, S.O.; funding acquisition, Y.S. All authors have read and agreed to the published version of the manuscript.

**Funding:** This work was supported in part by the Japan Society for the Promotion of Science (JSPS) KAKENHI under grant 21K12135.

**Institutional Review Board Statement:** Not applicable.

**Informed Consent Statement:** Not applicable.

**Data Availability Statement:** The dataset used in this study will be available from the authors.

**Conflicts of Interest:** The authors declare no conflicts of interest.

## References

1. Taira, H.; Rocco, I.; Sedlar, J.; Okutomi, M.; Sivic, J.; Pajdla, T.; Sattler, T.; Torii, A. Is This the Right Place? Geometric-Semantic Pose Verification for Indoor Visual Localization. In Proceedings of the 2019 IEEE/CVF International Conference on Computer Vision (ICCV), Seoul, Republic of Korea, 27 October–2 November 2019; pp. 4372–4382. [\[CrossRef\]](#)
2. Hyeon, J.; Kim, J.; Doh, N. Pose Correction for Highly Accurate Visual Localization in Large-scale Indoor Spaces. In Proceedings of the 2021 IEEE/CVF International Conference on Computer Vision (ICCV), Virtually, 11–17 October 2021; pp. 15954–15963. [\[CrossRef\]](#)
3. Liu, W.; Jiang, H.; Jiang, G.; Liu, J.; Ma, X.; Jia, Y.; Xiao, F. Indoor Navigation With Virtual Graph Representation: Exploiting Peak Intensities of Unmodulated Luminaries. *IEEE/ACM Trans. Netw.* **2019**, *27*, 187–200. [\[CrossRef\]](#)
4. Subbu, K.P.; Gozick, B.; Dantu, R. LocateMe: Magnetic-Fields-Based Indoor Localization Using Smartphones. *ACM Trans. Intell. Syst. Technol.* **2013**, *4*. [\[CrossRef\]](#)
5. He, S.; Chan, S.H.G. Wi-Fi Fingerprint-Based Indoor Positioning: Recent Advances and Comparisons. *IEEE Commun. Surv. Tutor.* **2016**, *18*, 466–490. [\[CrossRef\]](#)
6. Faragher, R.; Harle, R. Location Fingerprinting With Bluetooth Low Energy Beacons. *IEEE J. Sel. Areas Commun.* **2015**, *33*, 2418–2428. [\[CrossRef\]](#)
7. Tonosaki, K.; Sugaya, Y.; Miyazaki, T.; Omachi, S. Indoor Localization by Map Matching Using One Image of Guide Plate. In Proceedings of the Eighth International Conferences on Pervasive Patterns and Applications (PATTERNS 2016), Rome, Italy, 20–24 March 2016; pp. 22–26.
8. Kloch, K.; Lukowicz, P.; Fischer, C. Collaborative PDR Localisation with Mobile Phones. In Proceedings of the 2011 15th Annual International Symposium on Wearable Computers, San Francisco, CA, USA, 12–15 June 2011; pp. 37–40. [\[CrossRef\]](#)
9. Qiu, J.W.; Lin, C.P.; Tseng, Y.C. BLE-based collaborative indoor localization with adaptive multi-lateration and mobile encountering. In Proceedings of the 2016 IEEE Wireless Communications and Networking Conference, Doha, Qatar, 3–6 April 2016; pp. 1–7. [\[CrossRef\]](#)
10. Pratama, A.R.; Widyawan.; Hidayat, R. Smartphone-based Pedestrian Dead Reckoning as an indoor positioning system. In Proceedings of the 2012 International Conference on System Engineering and Technology (ICSET), Bandung, Indonesia, 11–12 September 2012; pp. 1–6. [\[CrossRef\]](#)
11. Kang, W.; Han, Y. SmartPDR: Smartphone-Based Pedestrian Dead Reckoning for Indoor Localization. *IEEE Sens. J.* **2015**, *15*, 2906–2916. [\[CrossRef\]](#)
12. Yan, H.; Shan, Q.; Furukawa, Y. RIDI: Robust IMU Double Integration. In Proceedings of the Computer Vision—ECCV 2018: 15th European Conference, Munich, Germany, 8–14 September 2018; Proceedings, Part XIII; Springer: Berlin/Heidelberg, Germany, 2018; pp. 641–656. [\[CrossRef\]](#)
13. Chen, C.; Lu, X.; Markham, A.; Trigoni, N. Ionet: Learning to cure the curse of drift in inertial odometry. In Proceedings of the AAAI Conference on Artificial Intelligence, New Orleans, LA, USA, 2–7 February 2018. [\[CrossRef\]](#)
14. Herath, S.; Yan, H.; Furukawa, Y. RoNIN: Robust Neural Inertial Navigation in the Wild: Benchmark, Evaluations, & New Methods. In Proceedings of the 2020 IEEE International Conference on Robotics and Automation (ICRA), Virtually, 31 May–31 August 2020; pp. 3146–3152. [\[CrossRef\]](#)
15. Liu, W.; Caruso, D.; Ilg, E.; Dong, J.; Mourikis, A.I.; Daniilidis, K.; Kumar, V.; Engel, J. TLIO: Tight Learned Inertial Odometry. *IEEE Robot. Autom. Lett.* **2020**, *5*, 5653–5660. [\[CrossRef\]](#)
16. Sun, S.; Melamed, D.; Kitani, K. IDOL: Inertial deep orientation-estimation and localization. In Proceedings of the AAAI Conference on Artificial Intelligence, Virtually, 2–9 February 2021; pp. 6128–6137. [\[CrossRef\]](#)
17. Herath, S.; Caruso, D.; Liu, C.; Chen, Y.; Furukawa, Y. Neural Inertial Localization. In Proceedings of the 2022 IEEE/CVF Conference on Computer Vision and Pattern Recognition (CVPR), New Orleans, LA, USA, 19–24 June 2022; pp. 6594–6603. [\[CrossRef\]](#)
18. Kaiser, S.; Khider, M.; Robertson, P. A maps-based angular PDF for navigation systems in indoor and outdoor environments. In Proceedings of the 2011 International Conference on Indoor Positioning and Indoor Navigation, Guimaraes, Portugal, 21–23 September 2011; pp. 1–7. [\[CrossRef\]](#)
19. Peng, C.; Weikersdorfer, D. Map As the Hidden Sensor: Fast Odometry-Based Global Localization. In Proceedings of the 2020 IEEE International Conference on Robotics and Automation (ICRA), Virtually, 31 May–31 August 2020; pp. 2317–2323. [\[CrossRef\]](#)
20. Rechy Rormero, A.; Borges, P.V.K.; Pfrunder, A.; Elfes, A. Map-Aware Particle Filter for Localization. In Proceedings of the 2018 IEEE International Conference on Robotics and Automation (ICRA), Brisbane, QLD, Australia, 21–25 May 2018; pp. 2940–2947. [\[CrossRef\]](#)
21. Melamed, D. Learnable Spatio-Temporal Map Embeddings for Deep Inertial Localization. Master’s Thesis, Carnegie Mellon University, Pittsburgh, PA, USA, 2021.
22. Peneda, L.; Azenha, A.; Carvalho, A. Trilateration for indoors positioning within the framework of wireless communications. In Proceedings of the 2009 35th Annual Conference of IEEE Industrial Electronics, Porto, Portugal, 3–5 November 2009; pp. 2732–2737. [\[CrossRef\]](#)
23. Xiong, J.; Jamieson, K. ArrayTrack: A Fine-Grained Indoor Location System. In Proceedings of the 10th USENIX Conference on Networked Systems Design and Implementation, Lombard, IL, USA, 2–5 April 2013; nsdi’13; pp. 71–84. [\[CrossRef\]](#)



24. Zampella, F.; Jiménez Ruiz, A.R.; Seco Granja, F. Indoor Positioning Using Efficient Map Matching, RSS Measurements, and an Improved Motion Model. *IEEE Trans. Veh. Technol.* **2015**, *64*, 1304–1317. [[CrossRef](#)]
25. Ascher, C.; Kessler, C.; Wankerl, M.; Trommer, G. Dual IMU Indoor Navigation with particle filter based map-matching on a smartphone. In Proceedings of the 2010 International Conference on Indoor Positioning and Indoor Navigation, Zurich, Switzerland, 15–17 September 2010; pp. 1–5. [[CrossRef](#)]
26. Woodman, O.; Harle, R. Pedestrian Localisation for Indoor Environments. In Proceedings of the 10th International Conference on Ubiquitous Computing, Seoul, Korea, 21–24 September 2008; Association for Computing Machinery: New York, NY, USA, 2008; UbiComp '08; pp. 114–123. [[CrossRef](#)]
27. Jinan, R.; Raveendran, T. Particle Filters for Multiple Target Tracking. *Procedia Technol.* **2016**, *24*, 980–987. . [[CrossRef](#)]
28. Tao, X.; Tu, X.; Wu, H. A new development in magnetic particle tracking technology and its application in a sheared dense granular flow. *Rev. Sci. Instrum.* **2019**, *90*, 065116. . [[CrossRef](#)] [[PubMed](#)]
29. Hu, C.; Li, M.; Song, S.; Yang, W.; Zhang, R.; Meng, M.Q.H. A Cubic 3-Axis Magnetic Sensor Array for Wirelessly Tracking Magnet Position and Orientation. *IEEE Sens. J.* **2010**, *10*, 903–913. [[CrossRef](#)]
30. Kalman, R.E. A New Approach to Linear Filtering and Prediction Problems. *J. Basic Eng.* **1960**, *82*, 35–45.
31. Chen, Z. Bayesian Filtering: From Kalman Filters to Particle Filters, and Beyond. *Statistics* **2003**, *182*. [[CrossRef](#)]
32. Filippopolitis, A.; Oliff, W.; Loukas, G. Bluetooth Low Energy Based Occupancy Detection for Emergency Management. In Proceedings of the 2016 15th International Conference on Ubiquitous Computing and Communications and 2016 International Symposium on Cyberspace and Security (IUCC-CSS), Granada, Spain, 14–16 December 2016; pp. 31–38. [[CrossRef](#)]
33. Tekler, Z.D.; Low, R.; Blessing, L. An alternative approach to monitor occupancy using bluetooth low energy technology in an office environment. *J. Phys. Conf. Ser.* **2019**, *1343*, 012116. [[CrossRef](#)]
34. Collotta, M.; Pau, G. A Novel Energy Management Approach for Smart Homes Using Bluetooth Low Energy. *IEEE J. Sel. Areas Commun.* **2015**, *33*, 2988–2996. [[CrossRef](#)]
35. Tekler, Z.D.; Low, R.; Yuen, C.; Blessing, L. Plug-Mate: An IoT-based occupancy-driven plug load management system in smart buildings. *Build. Environ.* **2022**, *223*, 109472. . [[CrossRef](#)]
36. Nguyen-Huu, K.; Lee, K.; Lee, S.W. An indoor positioning system using pedestrian dead reckoning with WiFi and map-matching aided. In Proceedings of the 2017 International Conference on Indoor Positioning and Indoor Navigation (IPIN), Sapporo, Japan, 18–21 September 2017; pp. 1–8. [[CrossRef](#)]
37. Sakoe, H.; Chiba, S. Dynamic programming algorithm optimization for spoken word recognition. *IEEE Trans. Acoust. Speech Signal Process.* **1978**, *26*, 43–49. [[CrossRef](#)]
38. Ke, G.; Meng, Q.; Finley, T.; Wang, T.; Chen, W.; Ma, W.; Ye, Q.; Liu, T.Y. LightGBM: A Highly Efficient Gradient Boosting Decision Tree. In *Advances in Neural Information Processing Systems*; Guyon, I., Luxburg, U.V., Bengio, S., Wallach, H., Fergus, R., Vishwanathan, S., Garnett, R., Eds.; Curran Associates, Inc.: Sydney, Australia, 2017; Volume 30.
39. Sipper, M. Binary and Multinomial Classification through Evolutionary Symbolic Regression. In Proceedings of the Genetic and Evolutionary Computation Conference Companion, Boston, MA, USA, 9–13 July 2022; Association for Computing Machinery: New York, NY, USA, 2022; GECCO '22; pp. 300–303. [[CrossRef](#)]
40. Qin, G.; Qin, G. Virtual Reality Video Image Classification Based on Texture Features. *Complexity* **2021**, *2021*, 5562136. . [[CrossRef](#)]
41. Li, P. Robust Logitboost and Adaptive Base Class (ABC) Logitboost. In Proceedings of the Twenty-Sixth Conference on Uncertainty in Artificial Intelligence, Catalina Island, CA, USA, 8–11 July 2010; AUAI Press: Arlington, VA, USA, 2010; UAI'10; pp. 302–311.
42. Tao, P.; Shen, H.; Zhang, Y.; Ren, P.; Zhao, J.; Jia, Y. Status Forecast and Fault Classification of Smart Meters Using LightGBM Algorithm Improved by Random Forest. *Wirel. Commun. Mob. Comput.* **2022**, *2022*, 3846637. . [[CrossRef](#)]
43. Long, J.; Shelhamer, E.; Darrell, T. Fully convolutional networks for semantic segmentation. In Proceedings of the 2015 IEEE Conference on Computer Vision and Pattern Recognition (CVPR), Boston, MA, USA, 7–12 June 2015; pp. 3431–3440. [[CrossRef](#)]
44. Chen, L.C.; Zhu, Y.; Papandreou, G.; Schroff, F.; Adam, H. Encoder-Decoder with Atrous Separable Convolution for Semantic Image Segmentation. In *Computer Vision—ECCV 2018*; Ferrari, V., Hebert, M., Sminchisescu, C., Weiss, Y., Eds.; Springer : Cham, Switzerland, 2018; pp. 833–851.

**Disclaimer/Publisher's Note:** The statements, opinions and data contained in all publications are solely those of the individual author(s) and contributor(s) and not of MDPI and/or the editor(s). MDPI and/or the editor(s) disclaim responsibility for any injury to people or property resulting from any ideas, methods, instructions or products referred to in the content.